remote sensing

MDPI

Article

Three-Dimensional Body and Centre of Mass Kinematics in Alpine Ski Racing Using Differential GNSS and Inertial Sensors

Benedikt Fasel [1], Jörg Spörri [2], Matthias Gilgien [3], Geo Boffi [1,4], Julien Chardonnens [1], Erich Müller [2] and Kamiar Aminian [1,*]

1 Laboratory of Movement Analysis and Measurement, Ecole Polytechnique Fédérale de Lausanne, 1015 Lausanne, Switzerland; benedikt.fasel@epfl.ch (B.F.); geo.boffi@geod.baug.ethz.ch (G.B.); julien.chardonnens@gmail.com (J.C.)

2 Department of Sport Science and Kinesiology, University of Salzburg, 5400 Hallein-Rif, Austria; joerg.spoerri@sbg.ac.at (J.S.); erich.mueller@sbg.ac.at (E.M.)

3 Department of Physical Performance, Norwegian School of Sport Sciences, 0806 Oslo, Norway; matthias.gilgien@nih.no

4 Institute of Geodesy and Photogrammetry, ETH Zurich, 8093 Zurich, Switzerland

* Correspondence: kamiar.aminian@epfl.ch; Tel.: +41-21-693-26-17

Academic Editors: Richard Müller and Prasad S. Thenkabail
Received: 30 June 2016; Accepted: 16 August 2016; Published: 22 August 2016

Abstract: A key point in human movement analysis is measuring the trajectory of a person's center of mass (CoM). For outdoor applications, differential Global Navigation Satellite Systems (GNSS) can be used for tracking persons since they allow measuring the trajectory and speed of the GNSS antenna with centimeter accuracy. However, the antenna cannot be placed exactly at the person's CoM, but rather on the head or upper back. Thus, a model is needed to relate the measured antenna trajectory to the CoM trajectory. In this paper we propose to estimate the person's posture based on measurements obtained from inertial sensors. From this estimated posture the CoM is computed relative to the antenna position and finally fused with the GNSS trajectory information to obtain the absolute CoM trajectory. In a biomechanical field experiment, the method has been applied to alpine ski racing and validated against a camera-based stereo photogrammetric system. CoM position accuracy and precision was found to be 0.08 m and 0.04 m, respectively. CoM speed accuracy and precision was 0.04 m/s and 0.14 m/s, respectively. The observed accuracy and precision might be sufficient for measuring performance- or equipment-related trajectory differences in alpine ski racing. Moreover, the CoM estimation was not based on a movement-specific model and could be used for other skiing disciplines or sports as well.

Keywords: inertial sensors; GNSS; sensor fusion; wearable system; skiing; center of mass; biomechanics

1. Introduction

In the sport of alpine ski racing, precise data of the center of mass (CoM) position, speed and acceleration are indispensable for the purposes of performance analysis and injury prevention [1–9]. Early studies mainly used camera-based stereo photogrammetry to collect kinematic data on a ski-slope and to reconstruct the CoM kinematics [2,3,7,10–13]. However, despite advantages in measurement accuracy, these systems are complex to set up and need for time-consuming post processing due to manual digitization. Moreover, they are limited in capture volume, allowing the analysis of a short turn sequence only. With the ongoing miniaturization of electronics, it became possible to use global navigation satellite systems (GNSS) in alpine skiing research [9,13–24]. However, one disadvantage of these systems is that the exact CoM position in space and time cannot be measured directly, as

the GNSS antenna is mounted on the head or neck. Thus, modeling methods are needed to estimate the CoM position relative to the GNSS antenna and to find the absolute position of the CoM, as previously suggested by the authors of [13,14,25]. In these studies, the models were based on inverse pendulum using precise surveying of the snow surface. However, for abnormal skiing movements violating the model hypotheses (e.g., during moments of loss of balance) the estimated CoM kinematics may be wrong. Moreover, surveying the snow surface is time consuming and is only feasible for research applications, but not within regular training sessions. Alternatively, inertial sensors could be used to estimate the athlete's body segment orientations and posture over time [26]. In alpine skiing research, such an approach was already used to estimate the relative COM kinematics (e.g., the athlete's CoM kinematics with respect to the athlete's head), and fused with a GNSS, to estimate the CoM kinematics with respect to a fixed reference frame [18,19,27]. Although these studies specified the errors of each system independently, they did not validate their final results on snow using the gold standard camera-based stereo photogrammetry. Fasel et al. [28] used seven inertial sensors to estimate a relative CoM based on a seven segment body model. Relative distances between the CoM and ankle position were estimated and validated. However, they did not compute the absolute joint and CoM positions in space.

Therefore, the aims of this study were threefold: (1) to design a novel algorithm to estimate CoM kinematics based on the trajectory and speed data obtained from a differential GNSS (dGNSS) and body segment orientations obtained from seven inertial sensors; (2) to reduce the number of sensor and to design an alternative algorithm that bases on the dGNSS data and the orientation of the athlete's head and sternum only; (3) to validate these algorithms against a camera-based stereo photogrammetric system.

2. Materials and Methods

2.1. Protocol

The measurements took place on a giant slalom slope of 26° inclination. Eleven gates were positioned at a constant distance of 27 m with an 8-m offset (Figure 1A). The left turn around gate 7 was covered with the video-based reference system. Six European Cup level alpine ski athletes participated in the study. Each athlete skied the course two times. Informed written consent was obtained from each athlete. The protocol was approved by the University Ethics Committee of the Department of Sport Science and Kinesiology at the University of Salzburg.

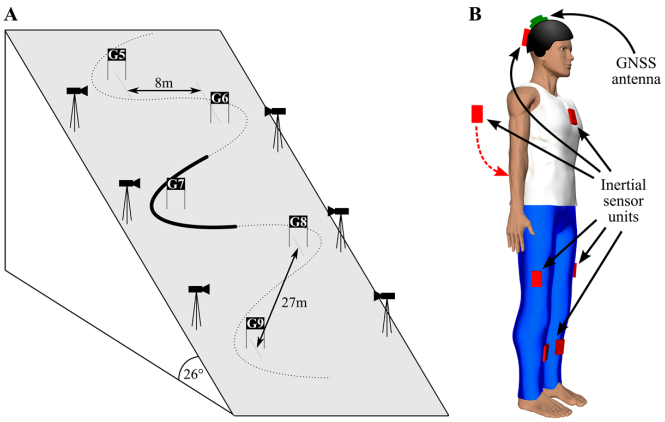

Figure 1. Materials and setup. (**A**) Illustration of the giant slalom slope. The left turn marked with the solid line was covered by the six cameras and analyzed in this study; (**B**) inertial sensors placed on both shanks and thighs, on the sacrum, sternum, and head. The global navigation satellite systems (GNSS) antenna was fixed to the athlete's helmet.

2.2. Wearable System

2.2.1. Inertial Sensors

Six inertial sensor units (Physilog® III, GaitUp, Renens, Switzerland) were placed on the left and right shank on the tibial plateau, above the ski boots, on the left and right thigh on the lateral side, mid-distance between the knee and hip joint center, on the sacrum and on the sternum using a custom made skin-tight underwear suit. A seventh inertial sensor unit was fixed to the athlete's helmet (Figure 1B). Three-dimensional acceleration and angular velocity were recorded on each sensor unit at 500 Hz. The sensors were wirelessly synchronized via radio (RF) synchronization pulses. Accelerometer offset and sensitivity was corrected as described in Reference [29]. Gyroscope offset was removed based on a static measurement before each run [30]. After functional calibration, initial sensor orientation was estimated based on the strapdown and drift-correction algorithm of Reference [31]. In a second step drift was further reduced by applying the method of the authors of [32] extended to 3D. The ISB standard convention [33] was used for the orientation of the segments' anatomical axes. Orientation accuracy and precision for alpine skiing was found to be in the order of 2° and 6°, respectively [34].

2.2.2. Differential Global Navigation Satellite System

Position and speed of the skiers head were tracked using dGNSS technology [15]. The GNSS antenna (G5Ant-2AT1, Torrance, AC, Canada) was fixed to the helmet to ensure optimal satellite visibility (Figure 1B) and the receiver (Alpha-G3T, Javad, San Jose, CA, USA), weighing 430 g, was placed in a backpack logging GPS and GLONASS signals using L1 and L2 frequency. Two reference stations equipped with antenna (GrAnt-G3T, Javad) and receiver (Alpha-G3T, Javad) logging GPS and GLONASS signals using frequency L1 and L2 were mounted on a tripod and placed close to the beginning of the race track (short baseline measurement). The reference base station's location was selected to reach the maximal number of satellites possible. The unit on the skier and base station recorded at a sampling frequency of 50 Hz. The antenna position and speed were computed in post processing applying kinematic carrier phase methods using geodetic software (Justin, Javad) as described in References [13,14]. The obtained position and speed were interpolated to 500 Hz using a spline filter to match the sampling frequency of the inertial sensors. The inertial sensors were electronically synchronized with the GNSS receiver using an electronic trigger.

The vertical axis of the dGNSS system and the inertial sensors was aligned using the Earth's gravity. The azimuth was aligned using the hypothesis that, on average, the left and right shanks' anterior–posterior anatomical axes were aligned with the skier's speed trajectory.

2.3. Centre of Mass Kinematics

The forward kinematic model proposed in Reference [35] was adapted to compute the CoM kinematics (i.e., position and speed) based on the GNSS antenna position and body segment orientations obtained with the inertial sensors. Two different models are proposed: the first model is based on a full 3D body model (Figure 2A), whereas the second model (Figure 2B) only used the orientations of the head and upper body to estimate the CoM kinematics. In both cases, first the relative position and speed of the CoM with respect to the GNSS antenna was estimated, and then added to the GNSS antenna position and speed to obtain the final, absolute estimate of CoM position and speed.

2.3.1. Full 3D Body Model

The full 3D body model was composed of the following segments: Head, upper trunk, lower trunk, left and right thigh, left and right shank, and arms. The weights of feet, boots, and skis were ignored. The weight of the GNSS system and clothing was assumed to be 1 kg, uniformly distributed on the trunk. The weight of the helmet was assumed constant at 0.5 kg. Segment inertial parameters

were taken in accordance with References [36,37] scaled for athletes' weights. It was assumed that the upper and lower trunk's weight was 40% and 60%, respectively, of the total weight of trunk and pelvis. All segment lengths were obtained from joint center position measurements from the reference system described in Reference [14]. Trunk joint center was defined to lie 0.05 m anterior and inferior of the middle of the trunk (i.e., the middle of the left/right hip and shoulder joints). Combining the segment lengths with their orientations allowed computing their 3D orientations and reconstructing the skier's posture (Equation (1)). The CoMs for the upper and lower trunk were supposed to be midway between trunk joint center and neck or hips, respectively. Since the arms' orientations were unknown, it was assumed that the CoM of both left and right arms combined was fixed with respect to the sternum and located 0.15 m anterior and 0.05 m superior to the trunk center (i.e., $\boldsymbol{d}_{trunk\ joint\ centre \rightarrow arms\ CoM} = [0.15\ 0.05\ 0]^T$, Figure 2A).

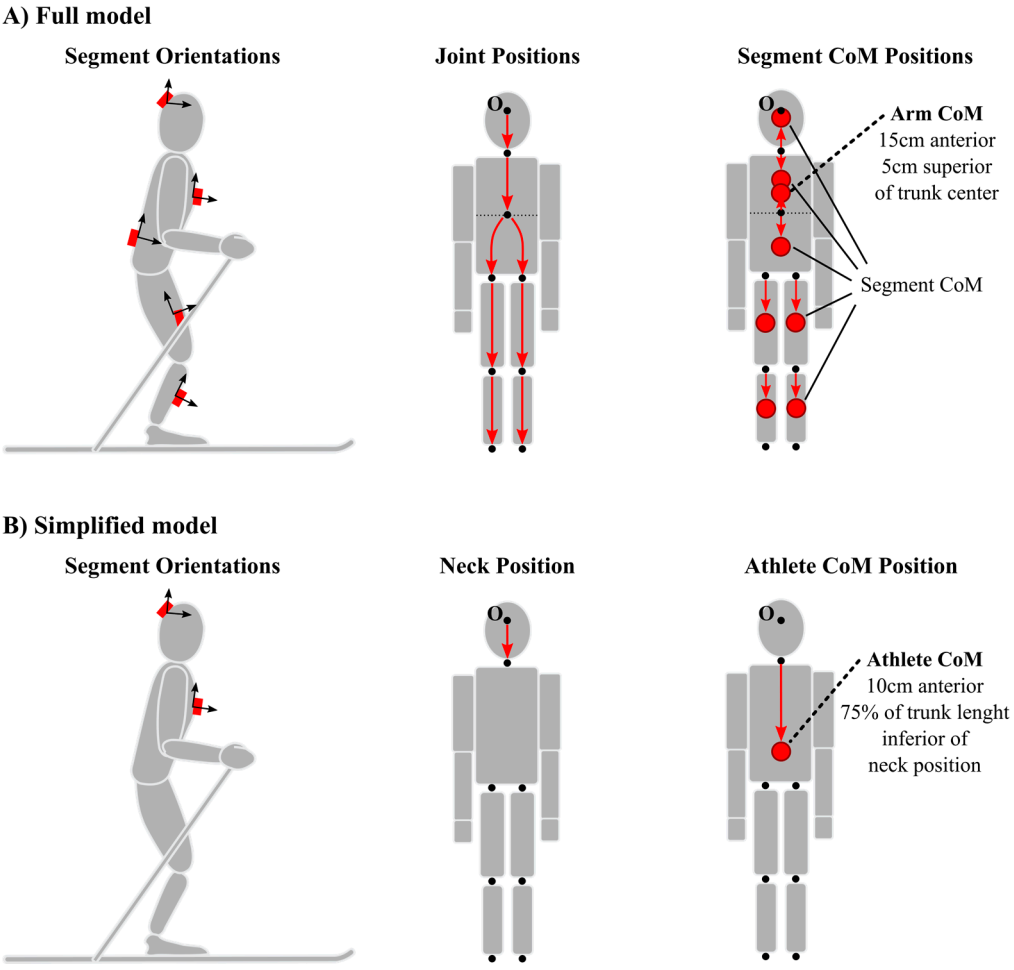

Figure 2. Kinematic chain used to compute the joint and segment CoM positions based on the segment orientations in the anatomical frame. (**A**) Full 3D body model based on all available inertial sensors; (**B**) simplified model based only on head and sternum inertial sensors.

In a first step, the joint positions for the neck, trunk center, left and right hip, left and right knee, and left and right ankle were computed based on Equation (1) (Figure 2A). The origin was defined to be at the GNSS antenna. In a second step, the positions for all segment COMs were computed based

on Equation (2) (Figure 2A). Based on all segments' COMs, the CoM of the athlete was estimated using a weighted sum (Equation (3)).

$$\begin{aligned}
\boldsymbol{p}_{neck} &= \boldsymbol{R}_{head}\, \boldsymbol{d}_{GNSS\rightarrow neck} \\
\boldsymbol{p}_{trunk\ joint\ centre} &= \boldsymbol{p}_{neck} + \boldsymbol{R}_{sternum}\, \boldsymbol{d}_{neck\rightarrow trunk\ joint\ centre} \\
\boldsymbol{p}_{left\ hip} &= \boldsymbol{p}_{trunk\ joint\ centre} + \boldsymbol{R}_{sacrum}\, \boldsymbol{d}_{trunk\ joint\ centre\rightarrow left\ hip} \\
\boldsymbol{p}_{right\ hip} &= \boldsymbol{p}_{trunk\ joint\ centre} + \boldsymbol{R}_{sacrum}\, \boldsymbol{d}_{trunk\ joint\ centre\rightarrow right\ hip} \\
\boldsymbol{p}_{left\ knee} &= \boldsymbol{p}_{left\ hip} + \boldsymbol{R}_{left\ thigh}\, \boldsymbol{d}_{left\ hip\rightarrow left\ knee} \\
\boldsymbol{p}_{right\ knee} &= \boldsymbol{p}_{right\ hip} + \boldsymbol{R}_{right\ thigh}\, \boldsymbol{d}_{right\ hip\rightarrow right\ knee} \\
\boldsymbol{p}_{left\ ankle} &= \boldsymbol{p}_{left\ knee} + \boldsymbol{R}_{left\ shank}\, \boldsymbol{d}_{left\ knee\rightarrow left\ ankle} \\
\boldsymbol{p}_{right\ ankle} &= \boldsymbol{p}_{right\ knee} + \boldsymbol{R}_{right\ shank}\, \boldsymbol{d}_{right\ knee\rightarrow right\ ankle}
\end{aligned} \tag{1}$$

where $\boldsymbol{p}_j$ is the position of the joint centre of joint j. $\boldsymbol{R}_s$ is the orientation matrix representing the orientation of segment s in the global frame, and $\boldsymbol{d}_{A\rightarrow B}$ is the vector connecting the joint A with B, expressed in the anatomical frame of segment connecting joint A with B.

$$\begin{aligned}
\boldsymbol{p}^{CoM}_{head} &= \boldsymbol{p}_{neck} + \boldsymbol{R}_{head}\, \boldsymbol{d}_{neck\rightarrow head\ CoM} \\
\boldsymbol{p}^{CoM}_{upper\ trunk} &= \boldsymbol{p}_{neck} + \boldsymbol{R}_{sternum}\, \boldsymbol{d}_{neck\rightarrow upper\ trunk\ CoM} \\
\boldsymbol{p}^{CoM}_{lower\ trunk} &= \boldsymbol{p}_{trunk\ joint\ centre} + \boldsymbol{R}_{sacrum}\, \boldsymbol{d}_{trunk\ joint\ centre\rightarrow lower\ trunk\ CoM} \\
\boldsymbol{p}^{CoM}_{arms} &= \boldsymbol{p}_{trunk\ joint\ centre} + \boldsymbol{R}_{sacrum}\, \boldsymbol{d}_{trunk\ joint\ centre\rightarrow arms\ CoM} \\
\boldsymbol{p}^{CoM}_{left\ thigh} &= \boldsymbol{p}_{left\ hip} + \boldsymbol{R}_{left\ thigh}\, \boldsymbol{d}_{left\ hip\rightarrow left\ thigh\ CoM} \\
\boldsymbol{p}^{CoM}_{right\ thigh} &= \boldsymbol{p}_{right\ hip} + \boldsymbol{R}_{right\ thigh}\, \boldsymbol{d}_{right\ hip\rightarrow right\ thigh\ CoM} \\
\boldsymbol{p}^{CoM}_{left\ shank} &= \boldsymbol{p}_{left\ knee} + \boldsymbol{R}_{left\ shank}\, \boldsymbol{d}_{left\ knee\rightarrow left\ shank\ CoM} \\
\boldsymbol{p}^{CoM}_{right\ shank} &= \boldsymbol{p}_{right\ knee} + \boldsymbol{R}_{right\ shank}\, \boldsymbol{d}_{right\ knee\rightarrow right\ shank\ CoM}
\end{aligned} \tag{2}$$

where $\boldsymbol{p}^{CoM}_s$ is the position of the CoM for segment s, $\boldsymbol{p}_j$ is the position of the joint center j, $\boldsymbol{R}_s$ is the orientation matrix representing the orientation of segment s in the global frame, and $\boldsymbol{d}_{A\rightarrow B}$ is the vector connecting the joint A with the CoM of the segment B, expressed in the anatomical frame of segment B.

$$\boldsymbol{p}^{CoM}_{athlete} = \frac{\sum_s m_s\, \boldsymbol{p}^{CoM}_s}{\sum_s m_s} \tag{3}$$

where m_s is the mass of segment s and is the sum is computed over the eight segments defined in Equation (2).

The speed of the athlete's CoM is computed analogous to the position (Equations (4)–(6)).

$$\begin{aligned}
\boldsymbol{v}_{neck} &= \boldsymbol{v}_{GNSS} + (\boldsymbol{R}_{head}\, \omega_{head}) \times (\boldsymbol{R}_{head}\, \boldsymbol{d}_{GNSS\rightarrow neck}) \\
\boldsymbol{v}_{trunk\ joint\ centre} &= \boldsymbol{v}_{neck} + (\boldsymbol{R}_{sternum}\, \omega_{sternum}) \\
&\quad \times \left(\boldsymbol{R}_{sternum}\, \boldsymbol{d}_{neck\rightarrow trunk\ joint\ centre}\right) \\
\boldsymbol{v}_{left\ hip} &= \boldsymbol{v}_{trunk\ joint\ centre} + (\boldsymbol{R}_{sacrum}\, \omega_{sacrum}) \\
&\quad \times \left(\boldsymbol{R}_{sacrum}\, \boldsymbol{d}_{trunk\ joint\ centre\rightarrow left\ hip}\right) \\
\boldsymbol{v}_{right\ hip} &= \boldsymbol{v}_{trunk\ joint\ centre} + (\boldsymbol{R}_{sacrum}\, \omega_{sacrum}) \\
&\quad \times \left(\boldsymbol{R}_{sacrum}\, \boldsymbol{d}_{trunk\ joint\ centre\rightarrow right\ hip}\right) \\
\boldsymbol{v}_{left\ knee} &= \boldsymbol{v}_{left\ hip} + \left(\boldsymbol{R}_{left\ thigh}\, \omega_{left\ thigh}\right) \times \left(\boldsymbol{R}_{left\ thigh}\, \boldsymbol{d}_{left\ hip\rightarrow left\ knee}\right) \\
\boldsymbol{v}_{right\ knee} &= \boldsymbol{v}_{right\ hip} + \left(\boldsymbol{R}_{right\ thigh}\, \omega_{right\ thigh}\right) \\
&\quad \times \left(\boldsymbol{R}_{right\ thigh}\, \boldsymbol{d}_{right\ hip\rightarrow right\ knee}\right)
\end{aligned} \tag{4}$$

$$
\begin{aligned}
\boldsymbol{v}_{head}^{CoM} &= \boldsymbol{v}_{neck} + (\boldsymbol{R}_{head}\,\boldsymbol{\omega}_{head}) \times (\boldsymbol{R}_{head}\,\boldsymbol{d}_{neck\rightarrow head\ CoM}) \\
\boldsymbol{v}_{upper\ trunk}^{CoM} &= \boldsymbol{v}_{neck} + (\boldsymbol{R}_{sternum}\,\boldsymbol{\omega}_{sternum}) \times \left(\boldsymbol{R}_{sternum}\,\boldsymbol{d}_{neck\rightarrow upper\ trunk\ CoM}\right) \\
\boldsymbol{v}_{lower\ trunk}^{CoM} &= \boldsymbol{v}_{trunk\ joint\ centre} + (\boldsymbol{R}_{sacrum}\,\boldsymbol{\omega}_{sacrum}) \\
&\quad \times \left(\boldsymbol{R}_{sacrum}\,\boldsymbol{d}_{trunk\ joint\ centre\rightarrow lower\ trunk\ CoM}\right) \\
\boldsymbol{v}_{arms}^{CoM} &= \boldsymbol{v}_{trunk\ joint\ centre} + (\boldsymbol{R}_{sacrum}\,\boldsymbol{\omega}_{sacrum}) \\
&\quad \times \left(\boldsymbol{R}_{sacrum}\,\boldsymbol{d}_{trunk\ joint\ centre\rightarrow arms\ CoM}\right) \\
\boldsymbol{v}_{left\ thigh}^{CoM} &= \boldsymbol{v}_{left\ hip} + \left(\boldsymbol{R}_{left\ thigh}\,\boldsymbol{\omega}_{left\ thigh}\right) \times \left(\boldsymbol{R}_{left\ thigh}\,\boldsymbol{d}_{left\ hip\rightarrow left\ thigh\ CoM}\right) \\
\boldsymbol{v}_{right\ thigh}^{CoM} &= \boldsymbol{v}_{right\ hip} + \left(\boldsymbol{R}_{right\ thigh}\,\boldsymbol{\omega}_{right\ thigh}\right) \\
&\quad \times \left(\boldsymbol{R}_{right\ thigh}\,\boldsymbol{d}_{right\ hip\rightarrow right\ thigh\ CoM}\right) \\
\boldsymbol{v}_{left\ shank}^{CoM} &= \boldsymbol{v}_{left\ knee} + \left(\boldsymbol{R}_{left\ shank}\,\boldsymbol{\omega}_{left\ shank}\right) \\
&\quad \times \left(\boldsymbol{R}_{left\ shank}\,\boldsymbol{d}_{left\ knee\rightarrow left\ shank\ CoM}\right) \\
\boldsymbol{v}_{right\ shank}^{CoM} &= \boldsymbol{v}_{right\ knee} + \left(\boldsymbol{R}_{right\ shank}\,\boldsymbol{\omega}_{right\ shank}\right) \\
&\quad \times \left(\boldsymbol{R}_{right\ shank}\,\boldsymbol{d}_{right\ knee\rightarrow right\ shank\ CoM}\right)
\end{aligned}
\tag{5}
$$

$$
\boldsymbol{v}_{athlete}^{CoM} = \frac{\sum_s m_s\,\boldsymbol{v}_s^{CoM}}{\sum_s m_s} \tag{6}
$$

where $\boldsymbol{v}_j$ is the speed at joint centre of joint j, $\boldsymbol{v}_{dGNSS}$ is the speed measured at the GNSS antenna, $\boldsymbol{v}_s^{CoM}$ is the speed of the *CoM* of segment s, $\boldsymbol{\omega}_s$ is the measured angular velocity in the segment s's anatomical frame, and $\boldsymbol{v}_{athlete}^{CoM}$ is the speed of the athlete's CoM.

2.3.2. Simplified Model

The above model was simplified to use only two sensors: Head and sternum. Thus, the body model consisted of one joint, the neck, connecting the two segments head and sternum. The athlete's CoM was fixed 0.1 m anterior and 75% of the trunk length (d_{trunk}, measured distance between shoulders and hips) inferior to the neck joint, i.e., $\boldsymbol{d}_{neck\rightarrow athlete\ CoM} = [0.1 - 0.75 d_{trunk}\ 0]^T$. The position and speed of the athlete's CoM were, therefore, computed according to Equations (7) and (8) (Figure 2B).

$$
\hat{\boldsymbol{p}}_{athlete}^{CoM} = \boldsymbol{p}_{dGNSS} + \boldsymbol{R}_{head}\,\boldsymbol{d}_{dGNSS\rightarrow neck} + \boldsymbol{R}_{sternum}\,\boldsymbol{d}_{neck\rightarrow athlete\ CoM} \tag{7}
$$

$$
\begin{aligned}
\hat{\boldsymbol{v}}_{athlete}^{CoM} &= \boldsymbol{v}_{dGNSS} + (\boldsymbol{R}_{head}\,\boldsymbol{\omega}_{head}) \times (\boldsymbol{R}_{head}\,\boldsymbol{d}_{dGNSS\rightarrow neck}) \\
&+ (\boldsymbol{R}_{sternum}\,\boldsymbol{\omega}_{sternum}) \times (\boldsymbol{R}_{sternum}\,\boldsymbol{d}_{neck\rightarrow athlete\ CoM})
\end{aligned}
\tag{8}
$$

where and $\boldsymbol{d}_{dGNSS\rightarrow neck}$ and $\boldsymbol{d}_{neck\rightarrow CoM}$ are the vectors connecting the dGNSS antenna position to the neck and the neck to the athlete's CoM, respectively.

2.4. Reference System

The reference system consisted of six gen-locked panned, tilted and zoomed HDV cameras (PMW-EX3, Sony, Tokyo, Japan) recording at 50 Hz, explained in detail in Reference [7]. Twenty-two joint centers and subject ambient reference points were manually digitized and reconstructed in 3D, as described in detail in References [7,14]. The mean resultant photogrammetric error of this methodology was reported to be 23 mm with a standard deviation of 10 mm [11]. The reconstructed joint center positions were then used to compute the athlete's CoM based on the body segment model of [36]. The reference system was synchronized with the inertial sensors using an electronic trigger. The reference system covered one entire left turn (Gate 7, solid black line Figure 1A).

2.5. Error Analysis

Each left turn at gate 7 was time normalized to 100 samples for both the wearable and reference system. Then, for each normalized turn and parameter, position error curves were defined as vector norm of the sample-by-sample difference between the wearable and reference system. Position error curves were computed for each joint center, the GNSS antenna position and the two CoM models. Speed error curves were defined as the difference of the speed norm between the wearable and reference system. Speed error curves were computed for the GNSS antenna and the two CoM models. For each run, median error and interquartile range were computed by averaging over time. The accuracy was computed as the median of all median errors and the precision as the median of the interquartile range.

3. Results

The proposed wearable system fused the data from the dGNSS with the inertial sensor-based system to obtain as accurate and precise position and speed estimates of the CoM as possible. Figure 3 shows the antenna position, reference CoM position, and $\boldsymbol{p}_{athlete}^{CoM}$ (A) and antenna speed, reference speed; and $\boldsymbol{v}_{athlete}^{CoM}$ (B) projected onto the horizontal plane (i.e., perpendicular to gravity) for three consecutive turns of a typical run. Figure 4 shows the average speed curves for the reference, full model and simplified model over the left turn at gate 7.

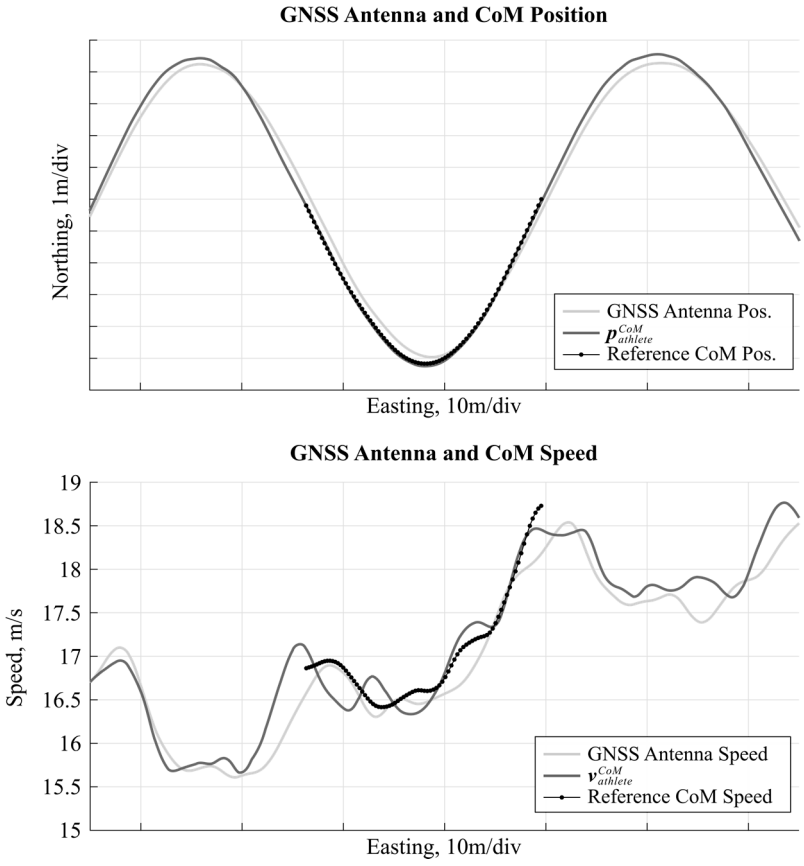

Figure 3. Position and speed curves for three consecutive turns (gates 6–8, Figure 1A) of a typical run. The central turn (gate 7) has been covered by the reference system. The athlete skied from left to right. (**Top**) GNSS antenna position (light grey), $\boldsymbol{p}_{athlete}^{CoM}$ (dark grey), and reference CoM position (dotted black) during the same turn. (**Bottom**) GNSS antenna speed (light grey), $\boldsymbol{v}_{athlete}^{CoM}$ (dark grey), and reference CoM speed (dotted black) during the same turn. Both figures are aligned such that their Easting axes are identical.

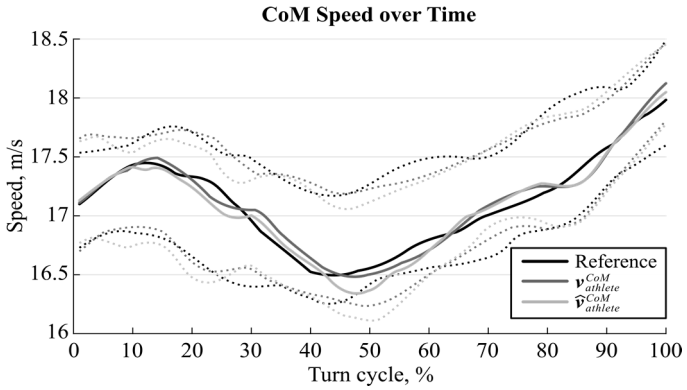

Figure 4. Reference speed (black) and estimated speed (dark and light grey) for the CoM. Solid lines are the median speed for all twelve turns at gate 7 analyzed and the dotted lines the 25th and 75th percentiles.

The GNSS antenna position error was on average (accuracy) 0.04 m with a standard deviation (precision) of 0.03 m (Table 1). The position difference between GNSS antenna and reference CoM was on average 0.62 m with a standard deviation of 0.05 m. The CoM model including the data obtained by inertial sensors allowed estimating this distance and correcting for it. After these corrections, the accuracy was found to be 0.08 m for $\boldsymbol{p}^{CoM}_{athlete}$ and 0.12 m for $\hat{\boldsymbol{p}}^{CoM}_{athlete}$, with a precision of 0.06 m (Table 1).

Table 1. Median accuracy and precision for all errors and differences between GNSS antenna and CoM speed and position.

Parameter	Accuracy (*Median* (*Median* (*E*)))	Precision (*Median* (*iqr* (*E*)))
Speed		
GNSS antenna speed error, m/s	−0.03	0.15
GNSS antenna—CoM speed difference, m/s	−0.15	0.20
$v^{CoM}_{athlete}$, m/s	0.04	0.14
$\hat{v}^{CoM}_{athlete}$, m/s	−0.01	0.14
Position		
GNSS antenna position error, m	0.04	0.03
GNSS antenna—CoM position difference, m	0.62	0.05
$p^{CoM}_{athlete}$, m	0.08	0.06
$\hat{p}^{CoM}_{athlete}$, m	0.12	0.06
Neck position error, m	0.06	0.03
Left hip position error, m	0.10	0.07
Right hip position error, m	0.10	0.07
Left knee position error, m	0.16	0.06
Right knee position error, m	0.14	0.08
Left ankle position error, m	0.17	0.07
Right ankle position error, m	0.15	0.09

With respect to the joint center positions of the full 3D body model, it can be observed that both accuracy and precision worsen the farther away the joint is from the GNSS antenna (Table 1). For $\boldsymbol{v}^{CoM}_{athlete}$ accuracy was found to be 0.04 m/s (0.24%) and precision 0.14 m/s (0.83%), respectively. $\hat{\boldsymbol{v}}^{CoM}_{athlete}$ had a similar accuracy (−0.01 m/s) and precision (0.14 m/s). Joint position errors, as well as the CoM position and CoM speed errors of the full 3D body and simplified model remained approximately constant over time (Figures 5 and 6).

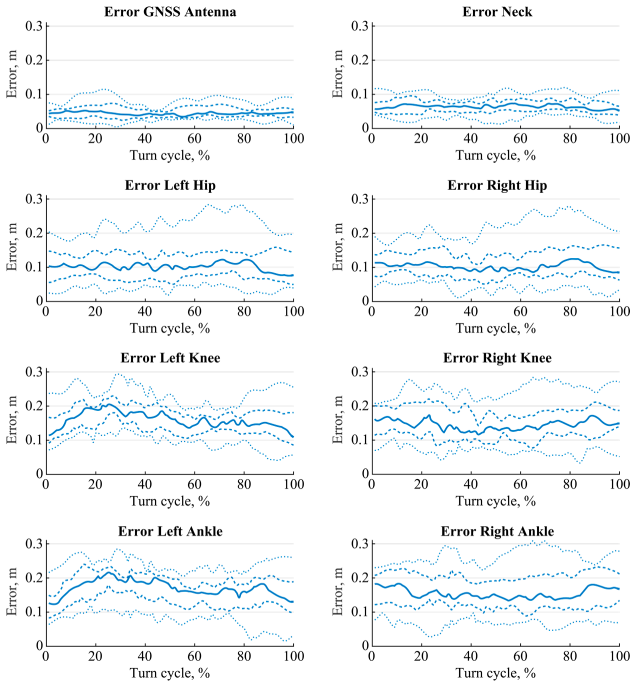

Figure 5. Position error of the GNSS antenna and the joint centers. In each graph the lines are, from bottom to top, the 5th (dotted), 25th (dashed), 50th (solid), 75th (dashed), and 95th (dotted) percentiles.

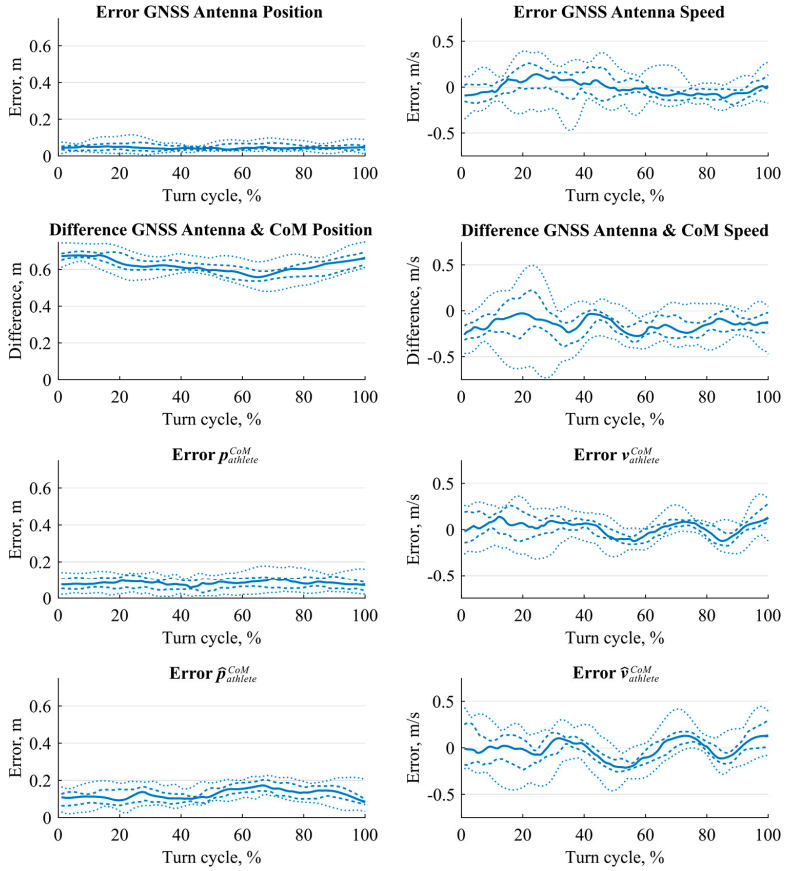

Figure 6. GNSS antenna position, speed and athlete CoM position, speed differences and errors. In each graph the lines are, from bottom to top, the 5th (dotted), 25th (dashed), 50th (solid), 75th (dashed), and 95th (dotted) percentiles.

4. Discussion

In the current study, dGNSS and inertial sensors have been combined for obtaining an estimate of the center of mass kinematics for alpine ski racing. In a first step, inertial sensors were used to compute a full 3D body model of the skier. In the second step, this model was fused with the position and speed data obtained from dGNSS and the skier's CoM kinematics were calculated. For an easy application in daily training, a simplified model using only two inertial sensors—fixed to the head and sternum—was proposed. Position errors were on average 0.08 m for the full 3D body model and 0.12 m for the simplified model. On average speed errors were found to be of the same order of magnitude for both models.

The proposed system's performance for measuring CoM position showed a similar accuracy (0.08 m compared to 0.09 m), but had a better precision (0.06 m compared to 0.12 m) than the inverted pendulum model proposed and validated by the authors of [14]. The advantage of the system proposed in the current study compared to the latter, was that no 3D terrain model was needed. However, instead, inertial sensors must be added to the dGNSS system. Medio-lateral motion (i.e., leaning inward)) was better measured by using inertial sensors (Figure 3), which may explain the better precision of the system proposed in the current study. This approach was based on a direct measurement of skiing movements and could also estimate speed and position during out-of-balance situations or jumps. When comparing the two systems, the system introduced by [14] was able to measure the overall CoM position with similar accuracy, but might have missed the full amplitude of the medio-lateral motion (inward leaning). By using a combination of both methods even better accuracy and precision values might be achieved for CoM position.

Interestingly, for the estimation of CoM speed, both the full 3D body and the simplified model had a similar accuracy and precision. This similarity in performance could be explained by the fact that the lower limbs have similar speed as the head and trunk segments and therefore have a low impact on overall CoM speed. As for the estimation of CoM position, the models were able to well measure the medio-lateral movements. Therefore, the system's speed accuracy and precision increased considerably compared to the case where speed measured at the GNSS antenna would have been used as the CoM speed. In Figures 3 and 4, it can be observed that the wearable speed estimation is oscillating around the reference speed (for both the average speed between all turns and the individual speed). One potential explanation of this measurement error might be that the wearable system is lacking information about the arm movements, which, perhaps, are used by the athlete to counterbalance small speed changes. When comparing individual runs instantaneous speed differences below 0.5 m/s, the approximate amplitude of the oscillations, might be caused by measurement errors. Comparing average speeds or accelerations over certain sections (e.g., turn phases) might, therefore, be advisable to reliably detect small speed changes below 0.5 m/s.

The individual joint position errors showed the typical error propagation characteristic of forward kinematic chains: the further the joint was along the chain the larger grew the errors, both for accuracy and precision (Figure 5 and Table 1). The accuracy decreased approximately 3–5 cm per joint except between the knee and ankle joints. Especially for the larger segment's orientation (as observed for the trunk or thigh segment), estimation errors of 2–3 degrees could cause errors of 2–3 cm in the estimation of the distal joint (e.g., hip and knee) position. These errors were then accumulated through the entire chain and did negatively affect the computation of CoM position. This error accumulation might also explain why the simple model reached almost the same accuracy and precision as the full 3D body model. On the other hand, this relatively small increase in joint position error towards more distal joints could also be an indication of accurate orientation estimate confirming the previously reported accuracy and precision in segment orientation estimation in the order of 2° and 6°, respectively [34].

Comparing the full 3D body with the simplified model it can be observed that the simplified model had a similar performance for both CoM position and speed. Thus, especially from a coaching perspective, the simplified system may be used. However, the full body 3D model has also its advantages: in addition to CoM position and speed the system could also deliver information about the

athlete's posture and joint kinematics, which then could be related to skiing performance. For instance, the full body 3D model would allow computing the distance between the ankle joint center and the athlete's CoM [28], an important performance-related parameter [2].

Earlier studies reported meaningful CoM speed differences of 0.5 m/s to 1 m/s within a slalom [2] and giant slalom [4] turn. Differences in the order of 0.5 m/s were also reported between turns of different course settings [4] or between the fastest and slowest trial of the same athlete and turn [3]. The accuracy and precision of the system proposed in this study was found to be approximately five times lower than the above differences between conditions. Consequently, the proposed systems' performance (both the full 3D body model and the simplified model) can be considered to be well suited for measuring such speed differences, although small meaningful differences might not always be detectable.

With regard to CoM line characteristics, Spörri et al. [3] reported differences in the order of 0.1 m to 0.5 m between fast and slow trials of the same athlete at the same course setting or between two different course settings. The proposed system's accuracy and precision of 0.08 m and 0.06 m might probably be just enough to detect larger differences in the skiers' CoM lines, as they can occur within the competition disciplines giant slalom, super-G, and downhill.

One limitation of the system proposed in this study is the fact that even the simplified system might be too complex to be used for performance analysis during everyday training. The handling of the dGNSS system with its reference base stations needs the presence of at least one additional person. Different approaches could be tried in order to increase the system's accuracy and reduce at the same time its complexity. In the current study the inertial data was processed entirely independent from the dGNSS data. In a future development sensor fusion approaches, such as Kalman and Particle filtering [38], could be applied to improve the GNSS trajectory information. In the same time, such a fusion method could also be used to further reduce drift in the estimation of the segment's orientation, increasing the body model's accuracy. To reduce the complexity the dGNSS system could also be replaced by a standard GNSS system not requiring any base stations. Further studies should address whether the loss of accuracy of standard GNSS compared to dGNSS could be compensated with the fusion of inertial sensor data.

5. Conclusions

This study provided the fundamental concepts for an accurate and precise estimation of a skier's CoM trajectory and speed based on the fusion of dGNSS and inertial sensors. Inertial sensor information was used to construct a body model to estimate relative CoM kinematics and was added to the absolute antenna kinematics obtained from a dGNSS. The proposed system was simpler to use than existing systems based on cameras or terrain models. Aiming an even simpler system, the reduction of sensors from a full 3D body model to a simplified trunk model lead to almost no decrease in accuracy and precision. The model's independency should allow to apply the algorithm without adaptations to the different skiing disciplines such as slalom or downhill. Future developments should aim at improving the accuracy and precision through better sensor fusion and at further simplifying the system.

Acknowledgments: This work was supported by the "Fondation de soutien à la recherche en orthopédie et traumatologie" and the Swiss Federal Office of Sport (FOSPO).

Author Contributions: Benedikt Fasel, Geo Boffi, Julien Chardonnens devised the algorithm. Jörg Spörri, Matthias Gilgien, Julien Chardonnens, Erich Müller, and Kamiar Aminian conceptualized the study design. Jörg Spörri, Matthias Gilgien, and Julien Chardonnens performed the biomechanical field experiments. Benedikt Fasel, Geo Boffi, Julien Chardonnens analyzed the inertial sensor data. Jörg Spörri processed and analyzed the data of the video-based reference system. Matthias Gilgien analyzed the dGNSS data. Benedikt Fasel wrote the paper with support, critical review, and final approvals from all co-authors.

Conflicts of Interest: The authors declare no conflict of interest.

References

1. Kröll, J.; Spörri, J.; Gilgien, M.; Chardonnens, J.; Müller, E. Verletzungsprävention innerhalb eines internationalen Sportverbandes—Eine Prozessbeschreibung am Beispiel des alpinen Skirennsports. *Sport Orthop. Traumatol.* **2013**. [CrossRef]
2. Reid, R.C. A Kinematic and Kinetic Study of Alpine Skiing Technique in Slalom. Ph.D. Thesis, Norwegian School of Sport Sciences, Oslo, Norway, 2010.
3. Spörri, J.; Kröll, J.; Schwameder, H.; Müller, E. Turn characteristics of a Top World Class Athlete in Giant Slalom: A case study assessing current performance prediction concepts. *Int. J. Sport Sci. Coach.* **2012**, *7*, 647–660. [CrossRef]
4. Spörri, J.; Kröll, J.; Schwameder, H.; Schiefermüller, C.; Müller, E. Course setting and selected biomechanical variables related to injury risk in alpine ski racing: An explorative case study. *Br. J. Sports Med.* **2012**, *46*, 1072–1077. [CrossRef] [PubMed]
5. Supej, M.; Kipp, R.; Holmberg, H.-C. Mechanical parameters as predictors of performance in alpine World Cup slalom racing. *Scand. J. Med. Sci. Sports* **2011**, *21*, e72–e81. [CrossRef] [PubMed]
6. Hébert-Losier, K.; Supej, M.; Holmberg, H.-C. Biomechanical factors influencing the performance of Elite Alpine Ski Racers. *Sport Med.* **2014**, *44*, 519–533. [CrossRef] [PubMed]
7. Spörri, J.; Kröll, J.; Gilgien, M.; Müller, E. Sidecut radius and the mechanics of turning—Equipment designed to reduce risk of severe traumatic knee injuries in alpine giant slalom ski racing. *Br. J. Sports Med.* **2016**, *50*, 14–19. [CrossRef] [PubMed]
8. Kröll, J.; Spörri, J.; Gilgien, M.; Schwameder, H.; Müller, E. Effect of ski geometry on aggressive ski behaviour and visual aesthetics: Equipment designed to reduce risk of severe traumatic knee injuries in Alpine Giant Slalom Ski Racing. *Br. J. Sports Med.* **2016**, *50*, 20–25. [CrossRef] [PubMed]
9. Kröll, J.; Spörri, J.; Gilgien, M.; Schwameder, H.; Müller, E. Sidecut radius and kinetic energy: Equipment designed to reduce risk of severe traumatic knee injuries in Alpine Giant Slalom Ski Racing. *Br. J. Sports Med.* **2016**, *50*, 26–31. [CrossRef] [PubMed]
10. Federolf, P.A. Quantifying instantaneous performance in alpine ski racing. *J. Sports Sci.* **2012**, *30*, 1063–1068. [CrossRef] [PubMed]
11. Klous, M.; Müller, E.; Schwameder, H. Collecting kinematic data on a ski/snowboard track with panning, tilting, and zooming cameras: Is there sufficient accuracy for a biomechanical analysis? *J. Sports Sci.* **2010**, *28*, 1345–1353. [CrossRef] [PubMed]
12. Supej, M.; Kugovnik, O.; Nemec, B. Kinematic determination of the beginning of a ski turn. *Kinesiol. Slov.* **2003**, *9*, 11–17.
13. Gilgien, M.; Spörri, J.; Chardonnens, J.; Kröll, J.; Müller, E. Determination of external forces in alpine skiing using a differential global navigation satellite system. *Sensors* **2013**, *13*, 9821–9835. [CrossRef] [PubMed]
14. Gilgien, M.; Spörri, J.; Chardonnens, J.; Kröll, J.; Limpach, P.; Müller, E. Determination of the centre of mass kinematics in alpine skiing using differential global navigation satellite systems. *J. Sports Sci.* **2015**, *33*, 960–969. [CrossRef] [PubMed]
15. Gilgien, M.; Spörri, J.; Limpach, P.; Geiger, A.; Müller, E. The effect of different Global Navigation Satellite System methods on positioning accuracy in Elite Alpine Skiing. *Sensors* **2014**, *14*, 18433–18453. [CrossRef] [PubMed]
16. Lachapelle, G.; Morrison, A.; Ong, R. Ultra-Precise positioning for sport applications. In Proceedings of the 13th IAIN World Congress, Stockholm, Sweden, 27–30 October 2009.
17. Waegli, A.; Skaloud, J. Optimization of two GPS/MEMS-IMU integration strategies with application to sports. *GPS Solut.* **2009**, *13*, 315–326. [CrossRef]
18. Supej, M. 3D measurements of alpine skiing with an inertial sensor motion capture suit and GNSS RTK system. *J. Sports Sci.* **2010**, *28*, 759–769. [CrossRef] [PubMed]
19. Brodie, M.; Walmsley, A.; Page, W. Fusion motion capture: A prototype system using inertial measurement units and GPS for the biomechanical analysis of ski racing. *Sport Technol.* **2008**, *1*, 17–28. [CrossRef]
20. Adelsberger, R.; Aufdenblatten, S.; Gilgien, M.; Tröster, G. On bending characteristics of skis in use. *Procedia Eng.* **2014**, *72*, 362–367. [CrossRef]

21. Gilgien, M.; Crivelli, P.; Spörri, J.; Kröll, J.; Müller, E. Correction: Characterization of course and terrain and their effect on skier speed in World Cup Alpine Ski Racing. *PLoS ONE* **2015**, *10*, e0128899. [CrossRef] [PubMed]
22. Gilgien, M.; Crivelli, P.; Spörri, J.; Kröll, J.; Müller, E. Characterization of Course and terrain and their effect on skier speed in World Cup Alpine Ski Racing. *PLoS ONE* **2015**, *10*, e0118119.
23. Gilgien, M.; Spörri, J.; Kröll, J.; Crivelli, P.; Müller, E. Mechanics of turning and jumping and skier speed are associated with injury risk in men's World Cup alpine skiing: A comparison between the competition disciplines. *Br. J. Sports Med.* **2014**, *48*, 742–747. [CrossRef] [PubMed]
24. Gilgien, M.; Spörri, J.; Kröll, J.; Müller, E. Effect of ski geometry and standing height on kinetic energy: Equipment designed to reduce risk of severe traumatic injuries in alpine downhill ski racing. *Br. J. Sports Med.* **2016**, *50*, 8–13. [CrossRef] [PubMed]
25. Supej, M.; Saetran, L.; Oggiano, L.; Ettema, G.; Šarabon, N.; Nemec, B.; Holmberg, H.-C. Aerodynamic drag is not the major determinant of performance during giant slalom skiing at the elite level. *Scand. J. Med. Sci. Sports* **2013**, *23*, e38–e47. [CrossRef] [PubMed]
26. Chardonnens, J.; Favre, J.; Cuendet, F.; Gremion, G.; Aminian, K. A system to measure the kinematics during the entire ski jump sequence using inertial sensors. *J. Biomech.* **2013**, *46*, 56–62. [CrossRef] [PubMed]
27. Krüger, A.; Edelmann-Nusser, J. Biomechanical analysis in freestyle snowboarding: Application of a full-body inertial measurement system and a bilateral insole measurement system. *Sport Technol.* **2009**, *2*, 17–23.
28. Fasel, B.; Spörri, J.; Kröll, J.; Müller, E.; Aminian, K. Using inertial sensors for reconstructing 3D full-body movement in sports—Possibilities and limitations on the example of Alpine Ski Racing. In Proceedings of the 33rd International Conference on Biomechanics in Sports, Poitiers, France, 29 June–3 July 2015.
29. Ferraris, F.; Grimaldi, U.; Parvis, M. Procedure for effortless in-field calibration of three-axis rate gyros and accelerometers. *Sens. Mater.* **1995**, *7*, 311–330.
30. Bergamini, E.; Ligorio, G.; Summa, A.; Vannozzi, G.; Cappozzo, A.; Sabatini, A.M. Estimating orientation using magnetic and inertial sensors and different sensor fusion approaches: Accuracy assessment in manual and locomotion tasks. *Sensors* **2014**, *14*, 18625–18649. [CrossRef] [PubMed]
31. Favre, J.; Jolles, B.M.; Siegrist, O.; Aminian, K. Quaternion-based fusion of gyroscopes and accelerometers to improve 3D angle measurement. *Electron. Lett.* **2006**, *42*, 612. [CrossRef]
32. Dejnabadi, H.; Jolles, B.M.; Casanova, E.; Fua, P.; Aminian, K. Estimation and visualization of sagittal kinematics of lower limbs orientation using body-fixed sensors. *IEEE Trans. Biomed. Eng.* **2006**, *53*, 1385–1393. [CrossRef] [PubMed]
33. Wu, G.; Cavanagh, P.R. ISB recommendations in the reporting for standardization of kinematic data. *J. Biomech.* **1995**, *28*, 1257–1261. [CrossRef]
34. Fasel, B.; Spörri, J.; Chardonnens, J.; Gilgien, M.; Kröll, J.; Müller, E.; Aminian, K. 3D measurement of lower limb kinematics in alpine ski racing using inertial sensors. In Proceedings of the 6th International Congress on Science and Skiing, St. Christoph am Arlberg, Austria, 14–19 December 2013.
35. Chardonnens, J.; Favre, J.; Cuendet, F.; Gremion, G.; Aminian, K. Measurement of the dynamics in ski jumping using a wearable inertial sensor-based system. *J. Sports Sci.* **2014**, *32*, 591–600. [CrossRef] [PubMed]
36. De Leva, P. Adjustments to Zatsiorsky-Seluyanov's segment inertia parameters. *J. Biomech.* **1996**, *29*, 1223–1230. [CrossRef]
37. Dumas, R.; Chèze, L.; Verriest, J.-P. Adjustments to McConville et al. and Young et al. body segment inertial parameters. *J. Biomech.* **2007**, *40*, 543–553. [CrossRef] [PubMed]
38. Won, S.H.P.; Melek, W.W.; Golnaraghi, F. A kalman/particle filter-based position and orientation estimation method using a position sensor/inertial measurement unit hybrid system. *IEEE Trans. Ind. Electron.* **2010**, *57*, 1787–1798. [CrossRef]